Published in final edited form as:

Cell Rep. 2017 March 14; 18(11): 2687–2701. doi:10.1016/j.celrep.2017.02.058.

Identification of Intrinsic Axon Growth Modulators for Intact CNS Neurons after Injury

Kathren L. Fink[1,4,5], **Francesc López-Giráldez**[2], **In-Jung Kim**[3,5], **Stephen M. Strittmatter**[1,4,5], and **William B.J. Cafferty**[1,6,*]

[1]Department of Neurology, Yale University School of Medicine, New Haven, CT 06520, USA

[2]Yale Center for Genome Analysis, Yale University School of Medicine, New Haven, CT 06520, USA

[3]Department of Ophthalmology, Yale University School of Medicine, New Haven, CT 06520, USA

[4]Program in Cellular Neuroscience, Neurodegeneration and Repair, Yale University School of Medicine, New Haven, CT 06520, USA

[5]Department of Neuroscience, Yale University School of Medicine, New Haven, CT 06520, USA

SUMMARY

Functional deficits persist after spinal cord injury (SCI) because axons in the adult mammalian central nervous system (CNS) fail to regenerate. However, modest levels of spontaneous functional recovery are typically observed after trauma and are thought to be mediated by the plasticity of intact circuitry. The mechanisms underlying intact circuit plasticity are not delineated. Here, we characterize the in vivo transcriptome of sprouting intact neurons from *Ngr1* null mice after partial SCI. We identify the lysophosphatidic acid signaling modulators LPPR1 and LPAR1 as intrinsic axon growth modulators for intact corticospinal motor neurons after adjacent injury. Furthermore, in vivo LPAR1 inhibition or LPPR1 overexpression enhances sprouting of intact corticospinal tract axons and yields greater functional recovery after unilateral brainstem lesion in wild-type mice. Thus, the transcriptional profile of injury-induced sprouting of intact neurons reveals targets for therapeutic enhancement of axon growth initiation and new synapse formation.

Graphical Abstract

*Correspondence: william.cafferty@yale.edu.
6Lead Contact

ACCESSION NUMBERS

The accession number for the raw sequencing data reported in this paper is NCBI GEO: GSE94482.

SUPPLEMENTAL INFORMATION

Supplemental Information includes Supplemental Experimental Procedures, seven figures, and four tables and can be found with this article online at http://dx.doi.org/10.1016/j.celrep.2017.02.058.

AUTHOR CONTRIBUTIONS

K.L.F., S.M.S., and W.B.J.C. designed experiments. K.L.F., F.L.-G., I.-J.K., and W.B.J.C. completed experiments. K.L.F., S.M.S., and W.B.J.C. wrote the paper.

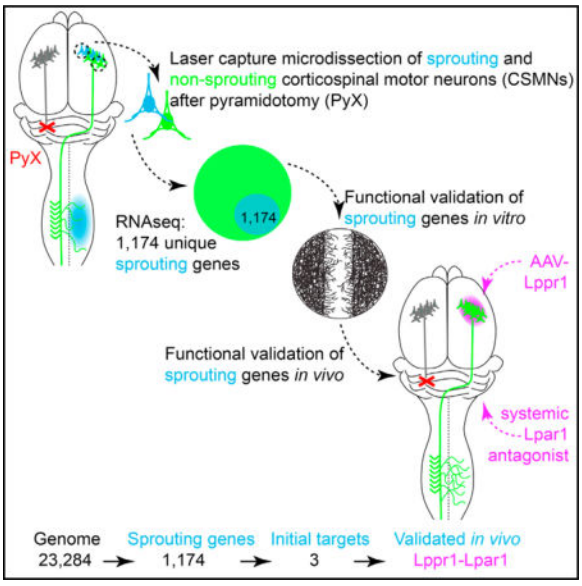

INTRODUCTION

Spinal cord injury (SCI) results in chronic functional deficits as axotomized adult CNS neurons fail to regenerate after trauma (He and Jin, 2016). Despite the lack of long distance axon regeneration, partial spontaneous recovery of function is observed in human SCI patients (Spiess et al., 2009) and in animal models (Basso et al., 1996). Structural plasticity of intact cortical, corticofugal, and spinal circuitry (Fink and Cafferty, 2016; Schwab and Strittmatter, 2014) has been suggested to drive this phenomenon. However, the molecular mechanisms underlying functional plasticity of intact circuits remain unknown. Identifying and exploiting such cell autonomous axon growth modulators would present an innovative direction for experimental SCI therapeutics. The corticospinal tract (CST) presents an opportunity to explore these mechanisms as it undergoes sprouting of intact axonal arbors across the spinal midline after unilateral lesion (pyramidotomy [PyX]). Strategies that enhance the intrinsic growth capacity of axotomized CST axons, such as inhibiting expression of phosphatase and tensin homolog (PTEN) (Liu et al., 2010) and overexpression of Kruppel-like factor 7 (KLF7) (Blackmore et al., 2012), SRY-related-HMG-box gene 11 (*Sox11*) (Wang et al., 2015), and signal transducer and activator of transcription 3 (STAT3) (Lang et al., 2013) also increase sprouting of intact CST axons post-PyX. Yet, these interventions fail to restore function robustly. In contrast, nullifying the activity of CNS inhibitors NOGOA, Nogo receptor 1 (NgR1), and chondroitin sulfate proteoglycans (CSPGs) not only stimulates intact CST axon sprouting, but also enhances functional recovery (Cafferty and Strittmatter, 2006; Starkey et al., 2012; Siegel et al., 2015) and adult brain plasticity (Akbik et al., 2013). These data suggest that such strategies utilize and/or reinforce the endogenous repair mechanisms that drive plasticity-mediated functional recovery.

To explore, we compared the transcriptomic profiles between adult intact “sprouting” corticospinal motor neurons (CSMNs) in an active growth mode with intact “quiescent”

CSMNs after PyX. This approach maximizes our capacity to identify the pro-axon growth transcriptomic signature of intact adult neurons by minimizing background gene expression "noise" due to developmental status (Blackmore et al., 2010), axotomy (Stam et al., 2007), and dissociation and cell culturing (MacGillavry et al., 2009). Additionally, screening within CNS neurons suggests that candidate therapies may be more efficacious in stimulating axon growth from refractory CNS neurons, rather than repurposing candidates identified from screening in peripheral sensory neurons (Chandran et al., 2016; Verhaagen et al., 2012). Here, we identify molecular factors that drive functional plasticity of intact adult CNS neurons after SCI.

RESULTS

Spinal Infusion of Fast Blue Labels Intact Sprouting CSMNs after PyX

Previously, we showed that *ngr1*$^{-/-}$ mice show a significant elevation in the number of intact CST axons that sprout functional arbors into the denervated side of the spinal cord after PyX (Cafferty and Strittmatter, 2006) compared to *ngr1*$^{+/+}$ controls. Thus, *plasticity sensitized ngr1*$^{-/-}$ mice present an opportunity to study the transcriptional profile of large numbers of intact sprouting CSMNs after partial SCI. *Crym*-GFP transgenic mice afford a ten times greater efficiency of CST labeling over extrinsic tracers (Fink et al., 2015), thus facilitating the exclusive identification of CSMNs for RNA sequencing (RNA-seq) analysis. To identify intact sprouting from intact quiescent CSMNs after PyX, we infused Fast Blue (FB) unilaterally into the denervated cervical cord 2 weeks after PyX and sham lesion in *ngr1*$^{-/-}$ and *ngr1*$^{+/+}$ *crym*-GFP mice (Figures 1A–1D, S1, and S2, herein referred to by genotype only).

Two weeks after FB infusion and 4 weeks after sham lesion, GFP^{+}FB^{+} CSMNs were seen in cortical layer V ipsilateral (ipsi) to the lesion in *ngr1*$^{+/+}$ and *ngr1*$^{-/-}$ mice (Figures S1B–S1E). There was no significant difference in the number FB^{+} CSMNs in ipsi cortex between genotypes (Figure 1F). Scarce GFP^{+}FB^{+} CSMNs were detected in contralateral (contra) cortex after sham lesion in both *ngr1*$^{+/+}$ and *ngr1*$^{-/-}$ mice (Figures S1B–S1E). These data confirm that the majority of CST axons terminate in contra spinal cord and our previous data, showing that CST wiring is identical between *ngr1*$^{-/-}$ and *ngr1*$^{+/+}$ mice (Fink et al., 2015). Four weeks after PyX, zero GFP^{+}FB^{+} CSMNs were observed in ipsi cortex in *ngr1*$^{+/+}$ and *ngr1*$^{-/-}$ (Figures 1C, S1G, and S1I). These data, in conjunction with the observation that the lesioned pyramidal tract is devoid of GFP^{+} CST axons in both *ngr1*$^{+/+}$ and *ngr1*$^{-/-}$ mice (Figures 1D, S1H, and S1J), confirms the accuracy of the PyX. Additionally, bilateral accumulation of FB in brainstem reticulospinal somata shows consistency of tracer transport between genotypes and lesions, as unlike the CST, the reticulospinal tract repeatedly crosses the midline and remains intact after PyX (Figures 1C, 1D, S1B, S1D, S1G, and S1I). In contrast to sham lesion, GFP^{+}FB^{+} CSMNs were detected in contra cortex in *ngr1*$^{+/+}$ mice (Figures S1G and S1H) 4 weeks after PyX. Furthermore, greater numbers of GFP^{+}FB^{+} CSMNs were detected in contra cortex in *ngr1*$^{-/-}$ (Figures 1C–1E, S1I, and S1J) versus *ngr1*$^{+/+}$ mice. In support, the denervated spinal cord revealed that significantly more intact GFP^{+} CST axons sprout in contra spinal gray matter in *ngr1*$^{-/-}$ compared to *ngr1*$^{+/+}$ mice 4 weeks after PyX (Figures S2A–S2G). Thus, FB^{+} somata in contra cortex represent the

population of intact CSMNs that have initiated an intrinsic growth program capable of supporting axon sprouting in contra spinal cord after PyX.

Intact Sprouting and Quiescent CSMNs Show Differential Gene Expression after PyX

Next, we sought to harvest CSMNs from intact and lesioned cortex to identify the transcriptomic signature driving intact circuit plasticity. We used laser capture microdissection (LCM) to collect intact control ($GFP^{-}FB^{-}$, Figure 2A, a′), intact quiescent CSMNs ($GFP^{+}FB^{-}$, Figure 2A, b′), and axotomized CSMNs ($GFP^{+}FB^{-}$, Figure 2A, c′) from *ngr1*$^{+/+}$ mice (n = 6) 4 weeks post-PyX, and intact control ($GFP^{-}FB^{-}$, Figure 2A, d′), intact quiescent CSMNs ($GFP^{+}FB^{-}$, Figure 2A, e′), intact sprouting CSMNs ($GFP^{+}FB^{+}$, Figure 2A, g′), and axotomized CSMNs ($GFP^{+}FB^{-}$, Figure 2A, f′) from *ngr1*$^{-/-}$ mice (n = 6) 4 weeks post-PyX (Table S1). Cells were then prepared for RNA- seq on the Illumina 2500 hiseq platform. As expected, scant numbers of $FB^{+}GFP^{+}$ CSMNs were observed in *ngr1*$^{+/+}$ mice, therefore adequate material for RNA extraction from intact sprouting CSMNs ($GFP^{+}FB^{+}$) was collected from *ngr1*$^{-/-}$ mice only. Aligned sequences (Trapnell et al., 2013) revealed an average sequencing depth of 52 million reads with 64.9% within coding regions (Table S2), comparable to cortical material sequenced after macro extraction (Han et al., 2009).

Hierarchical clustering (see the Experimental Procedures) revealed three major groupings (Figure 2B) with replicate samples (n = 3 genotype) clustering per cellular phenotype rather than genotype of origin. Group I included all non-CSMNs (GFP^{-}) from *ngr1*$^{+/+}$ and *ngr1*$^{-/-}$ mice. Group II included all intact and axotomized CSMNs ($GFP^{+}FB^{-}$) from *ngr1*$^{+/+}$ and *ngr1*$^{-/-}$ mice. Finally, group III, the most distantly related to all the other samples, included all intact sprouting CSMNs ($GFP^{+}FB^{+}$) from *ngr1*$^{-/-}$ mice (Figure 2B, magenta text). These data show that intact sprouting CSMNs display a unique gene expression profile compared to adjacent CSMNs in the same intact cortex, to axotomized CSMNs in the opposite cortex and non-CSMN material from the intact cortex in *ngr1*$^{-/-}$ mice, and an equally unique expression profile compared to intact and axotomized CSMNs and non-CSMNs from *ngr1*$^{+/+}$ mice. Accumulation of FB in these CSMNs shows they have mounted a significant growth response, and therefore the expression profile of these neurons should expose the molecular signature underlying this intrinsic growth response. Prior to exploring the biological import of significantly differentially expressed (SDE) genes in intact sprouting CSMNs, we sought to confirm the veracity of our strategy to collect discrete populations of axotomized and intact quiescent and sprouting CSMN samples. We wanted to confirm that our LCM samples were enriched in neuronal genes, known CSMN genes, and determine whether *Ngr1* deletion resulted in significant compensatory alterations in gene expression.

To test this, we compared gene expression between intact control non-CSMNs (GFP^{-}) and intact quiescent CSMNs (GFP+) from *ngr1*$^{+/+}$ (Figures 2C–2E) and *ngr1*$^{-/-}$ (Figures 2F–2H) mice. We found 674 genes (427 downregulated, 247 upregulated, Figure 2D) and 775 genes (546 downregulated, 229 upregulated, Figure 2G) were SDE in *ngr1*$^{+/+}$ and *ngr1*$^{-/-}$ mice, respectively. GFP^{+} samples were collected by laser capturing and pooling single CSMNs whereas GFP^{-} samples were collected as a contiguous area of cortex, therefore, we hypothesized GFP^{+} samples would reveal neuronal and CSMN enrichment. Indeed, intact

CSMNs (GFP^+) samples from $ngr1^{+l+}$ mice were enriched in neuronal genes including *Syt6, Nxph3, Sema5a, Grik3, Meg3,and Snhg11* (Zhang et al., 2014) and CSMN-specific genes including *Pcsk5* and *Crym* (Arlotta et al., 2005) with a dearth in expression of astrocytic genes including *Myom3, Prelp, Igfbp2, Ddit4l*, and *Ttpa* (Zhang et al., 2014)(Figure 2E; Table S3) compared to control non-CSMN samples (GFP^-) from $ngr1^{+l+}$ mice. Similarly, intact CSMNs (GFP^+) from $ngr1^{-/-}$ mice were enriched in neuronal genes including *Syt6, Foxo6, Ramp3, Sla*, and *Glra2* (Zhang et al., 2014) and CSMN-specific genes including *Pcsk5, Crym, Npr3, Cdh13,and Igfbp4* (Arlotta et al., 2005), with a dearth in expression of astrocytic genes such as *Tifa, Aass, Ttpa, Aldh1l1,and Prom1* (Zhang et al., 2014)(Figure 2H; Table S3) compared to control non-CSMN (GFP^-) samples from $ngr1^{-/-}$ mice. This confirms that *crym*-GFP specifically labels CSMNs, and LCM is an effective tool to enrich genomic material for a specific neuronal population.

To assess whether *Ngr1* deletion precipitated large-scale gene expression compensation, we compared expression between intact non-CSMNs (GFP^-, Figures 2I–2K) and intact CSMNs (GFP^+, Figures 2L–2N) between $ngr1^{+/+}$ and $ngr1^{-/-}$ mice. Only 25 genes (16 downregulated, 9 upregulated) were SDE between non-CSMNs (Figure 2J; Table S4), and 25 genes (22 downregulated, 3 upregulated) were SDE between intact CSMNs (Figure 2M; Table S4) between $ngr1^{+/+}$ and $ngr1^{-/-}$ mice, the clear majority remained unchanged (23, 259 genes). As expected, the most SDE gene between genotypes in both non-CSMN and CSMN samples was *ngr1* (*Rtn4r*, Figures 2K and 2N; Table S4). These data confirm deletion of *Ngr1*, and *Ngr1* deletion does not result in widespread genomic compensation in intact adult CNS neurons and glia in vivo. To test whether *ngr1* deletion influenced gene expression after in vivo perturbation, we compared expression between intact CSMNs and axotomized CSMNs in $ngr1^{+l+}$ and $ngr1^{-/-}$ mice. Only 42 genes (15 downregulated, 27 upregulated) were SDE in axotomized CSMNs in $ngr1^{+/+}$ mice (Figures 2O–2Q; Table S4) and 19 genes (8 downregulated, 11 upregulated) were SDE in axotomized CSMNs in $ngr1^{-/-}$ mice (Figures 2R and 2S; Table S4). Comparing expression profiles in axotomized CSMNs between $ngr1^{+l+}$ and $ngr1^{-/-}$ mice showed that only 87 genes (51 down-regulated, 36 upregulated) were SDE between genotypes (Figures S2H–S2J; Table S4). These data show that *ngr1* deletion exerts minimal influence upon axotomy-induced changes in CSMNs 4 weeks post-PyX.

Transcriptional Profile of Sprouting CSMNs Reveals Pathways that Facilitate Axon Growth

Next, we focused on comparing the transcriptional profile between intact sprouting CSMNs from $ngr1^{-/-}$ with intact quiescent CSMNs from $ngr1^{-/-}$ and $ngr1^{+l+}$ mice to specifically assess the molecular mechanisms driving plasticity within intact CNS neurons.

Gene expression analysis showed that 1,174 genes (112 downregulated, 1,062 upregulated) were SDE between intact sprouting CSMNs from $ngr1^{-/-}$ mice and intact quiescent CSMNs from $ngr1^{+/+}$ mice (Figures 3A–3C and 3I). A total of 1,092 genes (84 downregulated and 1,008 upregulated) were SDE between intact quiescent and intact sprouting CSMNs from $ngr1^{-/-}$ mice (Figures 3D–3F and 3J). Intact quiescent CSMNs from both $ngr1^{+l+}$ and $ngr1^{-/-}$ mice clustered together compared to intact sprouting CSMNs (Figures 3C and 3F), with 932 genes (242 unique to $ngr1^{+/+}$, 160 unique to $ngr1^{-/-}$) consistently SDE between

intact quiescent CSMNs in both genotypes versus intact sprouting CSMNs from *ngr1*$^{-/-}$ mice (Figure 3G). To gain biological insight into our list of SDE genes and to prioritize candidates for further investigation, we used a combination of functional significance algorithms and investigator supervised interrogation methods. Ingenuity pathway analysis (IPA) (https://www.qiagen.com/ingenuity) highlighted several pathways that were significantly enriched in sprouting CSMNs compared to quiescent CSMNs. The top three pathways in both comparisons included the HIPPO signaling pathway, mTOR signaling pathway, and the 3-phosphoinositide degradation pathway (Figure 3H, see also Table 1). mTOR has been shown to enhance axon regeneration and plasticity (Liu et al., 2010); therefore, we chose the HIPPO signaling and 3-phosphoinositide (PI) degradation pathways to probe for candidate genes. In addition to the pathway analysis, we also investigated the top SDE genes for functional relevance in the literature. The most downregulated gene observed in sprouting versus quiescent CSMNs was lysophosphatidic acid receptor 1 (*Lpar1*), moreover, more than 30 genes that interact with *Lpar1* were dysregulated in sprouting CSMNs (Table 1). Lysophosphatidic acid (LPA), the high-affinity ligand for LPAR1, is known to have effects in developmental axonal outgrowth (Choi et al., 2010). Based on these observations, we selected inositol polyphosphate-5-phosphatase K (*Inpp5k*) from the 3-phosphoinositide degradation pathway, WW domain containing transcription regulator 1, or TAZ (*Wwtr1*) from the HIPPO pathway, and lipid phosphate phospha-tase-related protein type 1 (*Lppr1*) from the *Lpar1* interacting pathway for functional validation in vitro and in vivo, as each was significantly upregulated in intact sprouting neurons and whose expression could be subsequently modulated via adeno-associated viral (AAV) delivery.

Overexpression of INPP5K and LPPR1 Enhances Neurite Outgrowth In Vitro

We used two in vitro models to assess the capacity of candidate genes to enhance axon growth (1) acute neurite outgrowth of dissociated cortical neurons, and (2) axon regeneration of mature cortical neurons after in vitro injury. Overexpression of INPP5K and LPPR1, but not TAZ, in E17.5 cortical neurons resulted in a significant increase in neurite outgrowth (Figures 4A and 4B). INPP5K overexpression significantly increased the number of processes and branches per neuron (Figures S3D and S3E), while LPPR1 overexpression significantly increased the number of branches per neuron (Figure S3E), and TAZ significantly decreased the number of processes per neuron (Figure S3D) after 3 days in vitro (DIV) compared to YFP transfected controls.

We identified candidate genes in intact sprouting adult neurons, which is poorly modeled with acute neurite outgrowth of embryonic neurons. Therefore, we used an additional in vitro model to assess the capacity of INPP5K and LPPR1 to increase axon growth in more mature cortical neuron cultures. TAZ was eliminated at this point as it failed to increase neurite outgrowth in acute cultures (Figure 4B). To this end, we cultured acutely dissociated E17.5 mouse cortical neurons transduced with AAV overexpressing INPP5K, LPPR1, or YFP control. At 14 DIV, a pin replicator was used to scrape the center of each well to induce an in vitro injury (Huebner et al., 2011), and 72 hr later, cultures were fixed, stained for β-tubulin, and scored for axon length of regenerating axons in the scrape zone (Figures 4C and 4D). Overexpression of INPP5K and LPPR1 increased regeneration of axons into the scrape

zone compared to controls (Figures 4C and 4D). The number of growth cones observed in the lesioned area was significantly elevated in LPPR1 over-expressing neurons (Figure S3F), consistent with an increase in the number of branches observed in acutely dissociated cortical neurons overexpressing LPPR1 after 7 DIV (Figure S3G). Next, we determined if LPPR1 accumulated in actin structures in cultured cortical neurons, thus predicting a role in neurite sprouting. After 7 DIV, LPPR1 overexpressing neurons exhibited elaborate branched neurite arbors compared to neurons expressing INPP5K or YFP (Figure S3G). V5-tagged LPPR1 accumulated in growth cones and actin-rich structures along cortical neurites (Figures 5A–5D). Accumulation in these structures points to a role for LPPR1 in mediating initiation and or elongation of neurites in vitro, suggesting that LPPR1 may also drive axon sprouting in vivo, thereby contributing to plasticity-induced functional recovery after PyX in intact CSMNs.

Modulation of LPAR1 Signaling Axis Enhances Sprouting after PyX In Vivo

Based on these neurite outgrowth data, together with our findings that *Lpar1* is significantly downregulated and *Lppr1* is significantly upregulated in intact sprouting neurons after PyX, we hypothesized that inhibiting LPAR1 signaling in intact CSMNs in vivo would enhance functional sprouting after PyX. To test this, we focused on targeting LPAR1 activation specifically in intact CSMNs by viral overexpression of LPPR1 and more broadly via systemic delivery of the LPAR1-specific antagonist AM095 (Figures 6A and 6B) (Swaney et al., 2011). To overex-press LPPR1 in vivo, custom AAVs were engineered to express V5-tagged LPPR1, or V5 control under a CAG promoter (Figures S3A and 3H–3U). AAV2/1-*Lppr1-V5* or AAV2/1-*V5* was co-infused with AAV2/1-*mCherry* into motor cortex of adult C57Bl6J mice (Figure 6B). Two weeks post-infusion, LPPR1 was detected specifically in cortex transduced with AAV-*Lppr1-V5* and showed extensive overlap with mCherry expression in ipsi cortex (Figures S3J–S3O). Coronal sections of cervical spinal cord showed LPPR1-V5 and mCherry co-expression in fasciculated CST axons in the ventral dorsal column projection, showing that LPPR1 and the reporter travel down CST axons and into CST collaterals in spinal gray matter (Figures S3P–S3U), mCherry fills the axons comprehensively and can be used as a surrogate for *Lppr1*-transduced CST axons. These data show that LPPR1 can be efficiently overexpressed in CSMNs in vivo and is present in the spinal cord by 2 weeks post-transduction.

Next, we completed PyX (Figures 6B and S4–S6) and sham lesion in adult C57BL/6J mice, which received either (a) cortical infusion of AAV-*Lppr1-V5* + vehicle (sham n = 7; PyX n = 15), (b) AAV-V5 + AM095 (sham n = 6; PyX n = 10), or (c) AAV-V5 + vehicle (sham n = 9; PyX n = 11). Viral infusions were conducted 2 weeks prior to lesion and oral drug/vehicle treatments began ~5 hr post-lesion and continued every 12 hr for 10 days post-lesion. All groups received cortical AAV-*mCherry* to label virally transduced CSMNs and localize CST axons in cervical spinal cord for histological analysis (Figures 6C–6H). To assess the functional impact of our treatments, all groups underwent grid walking analysis to assess fine motor function in both the fore and hind limbs (Figure 6K). All groups were sacrificed 4 weeks post-lesion after the last behavioral time point and prepared for histological analysis. To confirm PyX lesion completeness, cervical sections were stained with protein kinase C gamma (PKCγ)(Figures S4–S6) and mice with incomplete lesions were removed from all

analysis (Figure 6B, group a, AAV-*V5* + vehicle n = 1; group b, AAV-*Lppr1* + vehicle n = 0; and group c, AAV-V5 + AM095 n = 1, were removed from study).

Four weeks post-PyX and sham lesion, mCherry$^+$ CST axons were seen in the ventral dorsal columns and in spinal CST terminals contra to the reporter infusion site (intact side) in vehicle, LPPR1-treated, and AM095-treated mice (Figures 6C–6E and S4–S6). CST axon density was significantly elevated in the spinal ventral horn on the intact side in LPPR1- and AM095-treated mice compared to vehicle-treated sham-lesioned controls after both PyX and sham lesion (Figures 6F and S4–S6). CST axon density in the denervated ventral horn was elevated almost 10-fold in LPPR1-treated (Figures 6G, 6K, and S4–S6) and AM095-treated (Figures 6G, 6L, and S4–S6) mice after PyX in comparison to vehicle-treated sham-lesioned controls (Figure 6G). The number of CST axons crossing the midline normalized to the number of labeled CST axons in the intact dorsal columns was invariant between lesion and treatment (Figure 6H), confirming that the increase in CST terminal density in the denervated ventral horn was due to sprouting of resident CST axon arbors rather than labeling variability or increased midline crossing.

Grid-walking evaluation showed that sham-lesioned mice did not show a functional deficit post-lesion (Figures 6K and S7, solid lines), however, all PyX mice showed a significant deficit in contra (denervated) fore and hind limb motor function immediately post-lesion that incompletely resolved over time (Figures 6K and S7, stippled lines). The LPPR1-expressing mice exhibited a trend toward better recovery between days 14–28 post-injury, and the AM095-treated mice recovered significantly greater fore and hind limb function in comparison to vehicle-treated controls in the weeks after PyX (Figure 6K). To determine whether de novo CST sprouting was driving functional recovery in AM095-treated mice, we stained C6–C8 spinal cord sections with synaptophysin and NeuN. Many mCherry+ CST axons showed synaptophysin accumulation in areas contacting NeuN$^+$ structures in the denervated ventral horn (Figure 6J), suggesting the emergence of synapses between intact sprouting CST axons and denervated ventral horn neurons.

DISCUSSION

The current in vivo transcriptomic screening of intact functionally sprouting CSMNs after SCI demonstrates a key role in recovery in several regards. First, this methodology yields unique insight into the gene expression signature of a homotypic population of intact CNS neurons that are undergoing all phases of plasticity-mediated repair, including growth initiation, axon elongation, guidance, and functional synapse formation. To date, even the most potent pro-axon growth treatments produce little or no functional recovery (Geoffroy et al., 2016; Jin et al., 2015). Thus, exploiting the endogenous repair mechanisms identified in this screen may provide a more successful approach to therapeutic intervention. The current study focuses on genes that modulate axon growth, however, future studies can probe the dataset for initiators of synapse formation that can be combined with pro-axon growth treatments to maximize functional recovery after injury. Second, using this approach, we identify LPPR1 as a cell autonomous pro-axon growth modulator in adult neurons capable of driving sprouting of intact CSMNs after PyX. Third, we show that pharmacological inhibition of LPAR1 activation also stimulates sprouting of intact CSMNs after PyX and

thereby demonstrating bidirectional LPA axis regulation for beneficial axon growth. Fourth, significant restoration of fine motor function after AM095 treatment suggest that inhibiting LPAR1 may have a functional benefit for multiple intact spinal circuits, and additional candidates from our CSMN screen may support functional benefit across multiple CNS pathways.

Crym-GFP Affords Specificity for Cell Type-Specific Analysis

To maximize signal-to-noise, it was crucial to design an approach that identifies homotypic populations of intact quiescent and intact sprouting CSMNs after PyX. Traditionally, CSMNs are labeled by in vivo delivery of BDA (Tuszynski and Steward, 2012). However, for a genomic analysis, intra-cortical injections of BDA would be inefficient, non-specific, and would damage target somata. Therefore, we utilized *crym*-GFP transgenic mice to exclusively identify all populations of CSMNs (Fink et al., 2015). Therefore, using this transgenic line and delivering FB to the denervated side of the spinal cord after PyX, we could specifically identify and use LCM to extract intact sprouting CSMNs (GFP^+FB^+) and intact quiescent CSMNs (GFP^+FB^-) within the same cortical hemisphere for differential transcrip-tomic analysis. Profiling of GFP^+ CSMNs revealed an enrichment in neuronal and CSMN-specific genes (Arlotta et al., 2005), thus confirming the veracity of our intent to interrogate the transcriptional signature driving axon growth in intact CSMNs after PyX.

Previously, we reported that *Ngr1* null mice show increased CST axon sprouting into the denervated side of the spinal cord after PyX versus wild-type controls (Cafferty and Strittmatter, 2006). These data suggest that increased numbers of intact CSMNs had initiated a functional axon growth program in $ngr1^{-/-}$ mice after PyX. Here, we confirm this hypothesis as increased numbers of intact CSMNs contra to the PyX accumulate FB tracer in $ngr1^{-/-}$ compared to $ngr1^{+/+}$ mice. The absence of FB in contra cortex of sham mice indicates that the FB accumulating in CSMNs after PyX originates exclusively from intact CST axons that sprouted within the denervated spinal region infused with tracer. In support of our previous findings, significantly more CST axon arbors were seen sprouting in the denervated spinal cord in $ngr1^{-/-}$ compared to $ngr1^{+/+}$ mice (Figures S2A–S2G), thus supporting the finding of an increase in the number of FB^+ CSMNs observed in contra cortex after PyX. The increased sensitivity in CST axon labeling, afforded using the *crym*-GFP mice, allowed us to examine the full extent of CST axon sprouting after PyX. Intriguingly, we did not observe a difference in the number of GFP^+ CST axons crossing the spinal midline between $ngr1^{+/+}$ and $ngr1^{-/-}$ *crym*-GFP mice. Instead, we observed a significant increase in the density of CST innervation of the denervated ventral horn in $ngr1^{-/-}$ compared to $ngr1^{+/+}$ *crym*-GFP mice. These data suggest that BDA is grossly under-representing the extent of contra and ipsi spinal CST axon innervation before and after PyX. Indeed, a recent report that used a viral approach to fluorescently label CSMNs showed reporter expressing CST axons crossing the spinal midline in sham-lesioned control mice (Geoffroy et al., 2015). Furthermore, in this study, we observed manyCSTaxons transduced via cortical injection of AAV1-*mCherry* crossing the spinal midline in sham-lesioned vehicle-treated mice. Overex-pression of LPPR1 and delivery of the LPAR1-specific antagonist, AM095, did not result in an increase in the number of $mCherry^+$ CST axons crossing the midline, but rather both treatments increased the expansion of CST arbors deep

within the denervated ventral horn 4 weeks post-PyX. Crucially, many syn-aptophysin^{+} puncta were observed along mCherry^{+} sprouting CST axons. Therefore, studies that have used BDA to label CSMNs may be significantly underestimating the beneficial impact of treatments such as Chondroitinase ABC (Starkey et al., 2012), PTEN inhibition (Geoffroy et al., 2015; Liu et al., 2010), and KLF7 overexpression (Blackmore et al., 2012) on the sprouting of intact CST axons after PyX.

Specificity of In Vivo Screening Approach

Transcriptomic screening of intact CSMNs after PyX achieves an enhanced level of sensitivity that maximizes signal-to-noise to reveal cell autonomous modulators of CNS axon growth. Our approach has several advantages over previous screening experiments. First, this screen is conducted in vivo, in CNS neurons that can mount a growth response that drives functional recovery (Cafferty and Strittmatter, 2006). Numerous attempts have been made to identify intrinsic activators and inhibitors of CNS axon growth by screening dorsal root ganglion (DRG) neurons that have undergone peripheral nerve injury in vitro (Verhaagen et al., 2012) and in vivo (Chandran et al., 2016; Stam et al., 2007). DRGs are capable of robust regeneration after peripheral nerve injury and regeneration of the central processes of DRG neurons can be enhanced by prior peripheral nerve injury (Neumann and Woolf, 1999). Adult DRG neurons grow readily in culture while adult cortical neurons do not survive (Huebner et al., 2011), thus suggesting inherent differences in the fundamental growth capacity between DRG and CNS neurons. Accordingly, DRG screens have not yielded potent modulators of CNS axon growth (Chandran et al., 2016; Verhaagen et al., 2012). Here, we demonstrate that using candidate genes derived from screening adult CNS neurons can drive robust axon growth in CSMNs, which ultimately leads to functional benefit after SCI.

Alternative approaches to screen for axon-growth modulators have utilized embryonic cortical neurons in vitro. These approaches have successfully identified CNS axon growth enhancers including the KLF family of transcription factors and axon growth inhibitors including the phosphatase INPP5F (Blackmore et al., 2010; Zou et al., 2015). However, the full repertoire of intrinsic growth modulators cannot be easily revealed utilizing these approaches. For instance, cultured cortical neurons are inherently axotomized in the dissociation process; therefore, gene expression changes observed in vitro may predominantly be associated with injury rather than initiation of axon growth. Furthermore, axotomy upon dissociation also prohibits the identification of modulators of axon growth from intact neurons, thus limiting these studies to a focus on regeneration factors. The age of these cultured cortical neurons also poses challenges to screening for adult axon growth modulators. First, only embryonic stage neurons survive in numbers suitable for screening, thus restricting the utility of this model to identifying developmental growth modulators. Second, the immaturity of plated neurons restricts transcriptomic screening to a period in vitro prior to synapse formation (Huebner et al., 2011) and therefore cannot model functional axon growth that would be necessary to achieve functional recovery in vivo. Furthermore, these screens are conducted on permissive growth substrates such as laminin (Blackmore et al., 2010) or poly-D-lysine (Zou et al., 2015) that lack environmental inhibitors such as NOGOA and CSPGs and therefore, do not recapitulate the environmental

brakes on axon growth that are prevalent in the adult CNS. Here, we could overcome many of these in vitro restrictions and capture the transcriptional profile of adult neurons in vivo that are intact and undergoing a functional growth response in the CNS after SCI.

Intact Sprouting CSMNs Have Unique Transcriptomic Signature

Hierarchical clustering analysis revealed that the gene expression pattern in intact sprouting CSMNs 4 weeks post-PyX was most disparate when compared to intact quiescent CSMNs, axotomized CSMNs, and non-CSMN cortical controls (Figure 2B). Intact sprouting CSMNs were harvested from *ngr1*$^{-/-}$ *crym*-GFP mice only owing to scarcity in FB^{+} CSMNs detected in contra cortex of *ngr1*$^{+/+}$ *crym*-GFP mice during the LCM procedure. We detected minimal changes (on average <30 genes or ~0.1% of the genome) in the gene expression profile in non-CSMNs, intact quiescent CSMNs, and axotomized CSMNs between *ngr1*$^{+/+}$ and *ngr1*$^{-/-}$ *crym-GFP* mice, with *ngr1* the most downregulated gene between genotypes in all sample comparisons. These data suggest that *Ngr1* does not influence the development or homeostasis of the adult CST. We found that 1,174 and 1,092 genes were SDE between intact sprouting CSMNs from *ngr1*$^{-/-}$ mice and intact quiescent CSMNs from *ngr1*$^{+/+}$ and *ngr1*$^{-/-}$ mice respectively, with >85% of SDE genes shared between these comparisons. These data show that *Ngr1* does not influence the intrinsic growth state of adult intact CSMNs. Rather, loss of *Ngr1* simply removes an extrinsic brake on spontaneous plasticity, thus allowing more profuse growth of intact axons after SCI. The nature of the signal that initiates spontaneous growth from intact axons after SCI remains unknown, however, our identification of the gene expression profile driving intact CST circuit re-arrangement can be exploited to design innovative SCI therapeutics.

A recent collaborative effort suggested that identifying and promoting pathways and networks of genes involved in axon growth would be more functionally beneficial than identifying single candidate genes (Chandran et al., 2016). In line with this, we took a pathway approach to exploring our candidate gene list to identify modulators of axon growth. Drawing from the top enriched pathways, we selected *Inpp5k* and *Lppr1* as candidate genes that could potentially gate the 3-phosphoinostide degradation pathway and LPAR1 signaling pathways, respectively. In vitro investigation of these candidate genes showed that modulating LPAR1 signaling interactors increased both neurite length and branching and therefore posed the greatest potential benefit for promoting growth of intact axons in vivo after PyX.

LPPR1 Negatively Regulates LPAR1 Signaling to Promote Axon Growth

In support of our in vitro data showing increased axon growth upon overexpression of LPPR1, previous studies have shown that LPPR1 drives filopodial formation in neurons and accumulates in neurites and growth cones of embryonic hippocampal neurons in vitro (Velmans et al., 2013). LPPR1, also known as plasticity-related gene 3 (PRG3) was originally identified by sequence homology to the lipid phosphate phosphatases (LPPs) and PRG1 (Bräuer and Nitsch, 2008). PRG1/5 and LPPs dephosphorylate LPAto negatively regulate LPA signaling pathways (Broggini et al., 2010). Despite sequence homology in domains identified to mediate LPA dephosphorylation, evidence suggest that LPPR1 is unable to dephosphorylate LPA (Savaskan et al., 2004; Sigal et al., 2007). Nonetheless,

LPPR1 may still modulate LPA-LPA1 signaling by binding and sequestering LPA. LPA is significantly elevated after SCI (Santos-Nogueira et al., 2015), suggesting it could factor into diminished axon growth after CNS injury. LPA binding to LPAR1 is known to activate RhoA resulting in growth cone collapse in vitro (Kranenburg et al., 1997). These data, together with our findings that a negative regulator of LPA signaling, LPPR1, is upregulated and LPAR1 is downregulated in intact sprouting neurons, we hypothesized that inhibiting LPAR1 signaling in intact CSMNs would enhance functional sprouting after PyX. To test this, we focused on targeting LPAR1 activation specifically in intact CSMNs by viral overexpression of LPPR1 and more broadly via systemic delivery of the LPAR1-specific antagonist AM095. Previous reports have shown that pharmacological targeting ofLPAR1 activation modestly enhances functional recovery after SCI by blunting the post-injury immune response, reducing glial scarring, and enhancing the survival of oligodendrocytes (Goldshmit et al., 2012; Santos-Nogueira et al., 2015). Furthermore, transgenic overexpression of LPPR1 has been shown to incrementally increase regeneration of axotomized spinal axons (Broggini et al., 2016). In our model, the PyX lesion is located many spinal segments rostral to the anatomical loci driving functional changes, therefore glial scar-mediated effects are minimal in this model, thus isolating the effects of drug treatment to growth from intact axons. Accordingly, we confirmed that there is no increase in microglial activation after cortical LPPR1 expression or AM095 delivery compared to vehicle treatment (data not shown). Here, we demonstrate that overexpression of LPPR1 specifically in CSMNs or systemic blockade of LPAR1 enhances intact CST axon sprouting in the denervated side of the spinal cord, confirming a role for LPAR1 and LPA signaling in preventing plasticity of intact neurons after injury.

In sum, we utilize an in vivo transcriptomic screening approach to identify a set of pro-axon growth pathways capable of driving functional plasticity within intact spinal circuits after partial SCI. These data strongly a support a continued focus on comprehensively dissecting the molecular mechanisms that drive plasticity-mediated functional recovery after injury to maximally exploit their capacity to restore function after SCI.

EXPERIMENTAL PROCEDURES

Mice

BAC transgenic Tg(*crym*-EGFP)GF82Gsat mice, also known as *crym*-GFP mice as previously described (Fink et al., 2015), were procured from the GENSAT project (stock number 012003-UCD, The Gene Expression Nervous System Atlas [GENSAT] Project, NINDS contracts N01NS02331 and HSN271200723701C to The Rockefeller University, New York, NY) and backcrossed with C57BL/6 for nine generations. *Crym*-GFP mice were then crossed with *ngr1*$^{-/-}$ mice (Kim et al., 2004), subsequent *crym*-GFP *ngr1*$^{+/+}$ mice were crossed with non-transgenic *ngr1*$^{+/-}$ mice to create *crym*-GFP ngr1$^{+/+}$ and crym-GFP *ngr1*$^{-/-}$ mouse lines. Prior to behavioral assessment and surgery, mice were randomized and split into cages of three. These blocks were maintained unless evidence of fighting was apparent, upon which aggressors were singly housed.

For validation experiments, C57BL/6J were ordered from Jackson Laboratories. In order to minimize the number of animals used while maintaining enough rigor to achieve our

scientific objectives (Festing and Altman, 2002), we used freely available power analysis (http://Hedwig.mgh.harvard.edu/sample_size/js/js_parallel_quant.html) to estimate sample sizes. The experiments are powered at 90% based on the number of animals in each group, the SD as determined by previous forelimb behavioral data (Cafferty and Strittmatter, 2006) and a significance level of 0.05.

Surgery

All procedures and postoperative care were performed in accordance with the guidelines of the Institutional Animal Use and Care Committee (IACUC) at Yale University. Surgical procedures, unilateral pyramidotomy, intra-spinal Fast Blue (FB) injections, delivery of AM095 drug, and intracortical AAV infusions are detailed in the Supplemental Experimental Procedures.

Behavioral Analysis

Experimental mice used for in vivo validation of targets were assessed for skilled motor function using the grid-walking task (Starkey et al., 2005). Details are given in the Supplemental Experimental Procedures. Data are presented as the average percentage of impaired steps ± SEM. The Shapiro-Wilk test was used to assess whether data were normally distributed between groups at every time point studied. Subsequently, data were analyzed via repeated-measure ANOVA with Bonferroni's correction for multiple comparisons. Post hoc analysis was completed for statistically significant differences comparing the percentage of missteps at each time point between treatment groups and the effect of lesion over time with ANOVA.

Histology

Mice were euthanized with CO2 and were transcardially perfused with 0.9% NaCl (normal saline) followed by 4% PFA in PBS. Brains and spinal cords were dissected, post-fixed in 4% PFA overnight at 4°C, and subsequently embedded in 10% gelatin (Sigma Aldrich) dissolved in water for vibratome sectioning. Detailed immunohistological protocols and image analysis are provided in the Supplemental Experimental Procedures.

Laser Capture Microdissection, RNA-Seq, and Sequencing Analysis

Four weeks after PyX and 2 weeks after FB tracing, $ngr1^{+/+}$ (n = 6) and $ngr1^{-/-}$ (n = 6) *crym*-GFP mice were sacrificed with an overdose of CO_2 and prepared for laser capture microdissection (LCM). Total RNA was extracted, amplified, and underwent RNA-seq using standard Illumina protocols. Comprehensive extraction, RNA preparation, sequencing, and analysis are provided in the Supplemental Experimental Procedures.

AAV Production

AAVs were generated in house to overexpress candidate genes to test for a functional role in enhancing sprouting in vitro and in vivo. Comprehensive details of plasmid preparation and AAV synthesis are provided in the Supplemental Experimental Procedures.

Cortical Neuron Culture

Embryonic cortical neurons were cultured as described previously (Zou et al., 2015). Detailed protocols for acute dissociated cortical neuron out growth, cortical neuron scrape assay, and preparation of cortical neurons for western blotting are provided in the Supplemental Experimental Procedures.

Statistical Analysis

For comparisons between two groups, two-tailed t test assuming unequal variance was used. For comparison among three or more groups, one-way ANOVA was used to compare each group mean with the control group mean with Dunnett's correction for multiple comparisons. Measurements taken at different time points in two groups of mice were compared using one-way repeated-measure ANOVA, with post hoc test at specific times if the series was significantly different. Analyses were conducted using Excel, GraphPad Prism 6, and SPSS.

Supplementary Material

Refer to Web version on PubMed Central for supplementary material.

Acknowledgments

This work was supported by grants from the NIH and Craig H. Neilsen Foundation (to W.B.J.C), Wings for Life, and Falk Medical Research Trust (to S.M.S.). S.M.S. is a co-founder of Axerion Therapeutics, seeking to develop NgR1-based therapeutics for SCI.

References

Akbik FV, Bhagat SM, Patel PR, Cafferty WB, Strittmatter SM. Anatomical plasticity of adult brain is titrated by Nogo Receptor 1. Neuron. 2013; 77:859–866. [PubMed: 23473316]

Arlotta P, Molyneaux BJ, Chen J, Inoue J, Kominami R, Macklis JD. Neuronal subtype-specific genes that control corticospinal motor neuron development in vivo. Neuron. 2005; 45:207–221. [PubMed: 15664173]

Basso DM, Beattie MS, Bresnahan JC. Graded histological and locomotor outcomes after spinal cord contusion using the NYU weight-drop device versus transection. Exp Neurol. 1996; 139:244–256. [PubMed: 8654527]

Blackmore MG, Moore DL, Smith RP, Goldberg JL, Bixby JL, Lemmon VP. High content screening of cortical neurons identifies novel regulators of axon growth. Mol Cell Neurosci. 2010; 44:43–54. [PubMed: 20159039]

Blackmore MG, Wang Z, Lerch JK, Motti D, Zhang YP, Shields CB, Lee JK, Goldberg JL, Lemmon VP, Bixby JL. Krüppel-like Factor 7 engineered for transcriptional activation promotes axon regeneration in the adult corticospinal tract. Proc Natl Acad Sci USA. 2012; 109:7517–7522. [PubMed: 22529377]

Brauer AU, Nitsch R. Plasticity-related genes (PRGs/LRPs): a brain-specific class of lysophospholipid-modifying proteins. Biochim Bio-phys Acta. 2008; 1781:595–600.

Broggini T, Nitsch R, Savaskan NE. Plasticity-related gene 5 (PRG5) induces filopodia and neurite growth and impedes lysophosphatidic acid-and nogo-A-mediated axonal retraction. Mol Biol Cell. 2010; 21:521–537. [PubMed: 20032306]

Broggini T, Schnell L, Ghoochani A, Mateos JM, Buchfelder M, Wien-dieck K, Schäfer MK, Eyupoglu IY, Savaskan NE. Plasticity Related Gene 3 (PRG3) overcomes myelin-associated growth inhibition and promotes functional recovery after spinal cord injury. Aging (Albany NY). 2016; 8:2463–2487. [PubMed: 27744421]

Cafferty WB, Strittmatter SM. The Nogo-Nogo receptor pathway limits a spectrum of adult CNS axonal growth. J Neurosci. 2006; 26:12242–12250. [PubMed: 17122049]

Chandran V, Coppola G, Nawabi H, Omura T, Versano R, Huebner EA, Zhang A, Costigan M, Yekkirala A, Barrett L, et al. A systems-level analysis of the peripheral nerve intrinsic axonal growth program. Neuron. 2016; 89:956–970. [PubMed: 26898779]

Choi JW, Herr DR, Noguchi K, Yung YC, Lee CW, Mutoh T, Lin ME, Teo ST, Park KE, Mosley AN, Chun J. LPA receptors: subtypes and biological actions. Annu Rev Pharmacol Toxicol. 2010; 50:157–186. [PubMed: 20055701]

Festing MF, Altman DG. Guidelines for the design and statistical analysis of experiments using laboratory animals. ILAR J. 2002; 43:244–258. [PubMed: 12391400]

Fink KL, Cafferty WB. Reorganization of intact descending motor circuits to replace lost connections after injury. Neurotherapeutics. 2016; 13:370–381. [PubMed: 26846379]

Fink KL, Strittmatter SM, Cafferty WB. Comprehensive corticospinal labeling with mu-crystallin transgene reveals axon regeneration after spinal cord trauma in ngr1−/− mice. J Neurosci. 2015; 35:15403–15418. [PubMed: 26586827]

Geoffroy CG, Lorenzana AO, Kwan JP, Lin K, Ghassemi O, Ma A, Xu N, Creger D, Liu K, He Z, Zheng B. Effects of PTEN and Nogo codeletion on corticospinal axon sprouting and regeneration in mice. J Neurosci. 2015; 35:6413–6428. [PubMed: 25904793]

Geoffroy CG, Hilton BJ, Tetzlaff W, Zheng B. Evidence for an age-dependent decline in axon regeneration in the adult mammalian central nervous system. Cell Rep. 2016; 15:238–246. [PubMed: 27050519]

Goldshmit Y, Matteo R, Sztal T, Ellett F, Frisca F, Moreno K, Crombie D, Lieschke GJ, Currie PD, Sabbadini RA, Pébay A. Blockage of lysophosphatidic acid signaling improves spinal cord injury outcomes. Am J Pathol. 2012; 181:978–992. [PubMed: 22819724]

Han X, Wu X, Chung WY, Li T, Nekrutenko A, Altman NS, Chen G, Ma H. Transcriptome of embryonic and neonatal mouse cortex by high-throughput RNA sequencing. Proc Natl Acad Sci USA. 2009; 106:12741–12746. [PubMed: 19617558]

He Z, Jin Y. Intrinsic control of axon regeneration. Neuron. 2016; 90:437–451. [PubMed: 27151637]

Huebner EA, Kim BG, Duffy PJ, Brown RH, Strittmatter SM. A multi-domain fragment of Nogo-A protein is a potent inhibitor of cortical axon regeneration via Nogo receptor 1. J Biol Chem. 2011; 286:18026–18036. [PubMed: 21454605]

Jin D, Liu Y, Sun F, Wang X, Liu X, He Z. Restoration of skilled locomotion by sprouting corticospinal axons induced by co-deletion of PTEN and SOCS3. Nat Commun. 2015; 6:8074. [PubMed: 26598325]

Kim JE, Liu BP, Park JH, Strittmatter SM. Nogo-66 receptor prevents raphespinal and rubrospinal axon regeneration and limits functional recovery from spinal cord injury. Neuron. 2004; 44:439–451. [PubMed: 15504325]

Kranenburg O, Poland M, Gebbink M, Oomen L, Moolenaar WH. Dissociation of LPA-induced cytoskeletal contraction from stress fiber formation by differential localization of RhoA. J Cell Sci. 1997; 110:2417–2427. [PubMed: 9410880]

Kranenburg O, Poland M, van Horck FP, Drechsel D, Hall A, Moolenaar WH. Activation of RhoA by lysophosphatidic acid and Galpha12/13 subunits in neuronal cells: induction of neurite retraction. Mol Biol Cell. 1999; 10:1851–1857. [PubMed: 10359601]

Lang C, Bradley PM, Jacobi A, Kerschensteiner M, Bareyre FM. STAT3 promotes corticospinal remodelling and functional recovery after spinal cord injury. EMBO Rep. 2013; 14:931–937. [PubMed: 23928811]

Liu K, Lu Y, Lee JK, Samara R, Willenberg R, Sears-Kraxberger I, Tedeschi A, Park KK, Jin D, Cai B, et al. PTEN deletion enhances the regenerative ability of adult corticospinal neurons. Nat Neurosci. 2010; 13:1075–1081. [PubMed: 20694004]

MacGillavry HD, Stam FJ, Sassen MM, Kegel L, Hendriks WT, Verhaagen J, Smit AB, van Kesteren RE. NFIL3 and cAMP response element-binding protein form a transcriptional feedforward loop that controls neuronal regeneration-associated gene expression. J Neurosci. 2009; 29:15542–15550. [PubMed: 20007478]

Neumann S, Woolf CJ. Regeneration of dorsal column fibers into and beyond the lesion site following adult spinal cord injury. Neuron. 1999; 23:83–91. [PubMed: 10402195]

Santos-Nogueira E, López-Serrano C, Hernàndez J, Lago N, Astudillo AM, Balsinde J, Estivill-Torriús G, de Fonseca FR, Chun J, López-Vales R. Activation of lysophosphatidic acid receptor type 1 contributes to pathophysiology of spinal cord injury. J Neurosci. 2015; 35:10224–10235. [PubMed: 26180199]

Savaskan NE, Bräuer AU, Nitsch R. Molecular cloning and expression regulation of PRG-3, a new member of the plasticity-related gene family. Eur J Neurosci. 2004; 19:212–220. [PubMed: 14750979]

Schwab ME, Strittmatter SM. Nogo limits neural plasticity and recovery from injury. Curr Opin Neurobiol. 2014; 27:53–60. [PubMed: 24632308]

Siegel CS, Fink KL, Strittmatter SM, Cafferty WB. Plasticity of intact rubral projections mediates spontaneous recovery of function after corticospinal tract injury. J Neurosci. 2015; 35:1443–1457. [PubMed: 25632122]

Sigal YJ, Quintero OA, Cheney RE, Morris AJ. Cdc42 and ARP2/3-independent regulation of filopodia by an integral membrane lipid-phosphatase-related protein. J Cell Sci. 2007; 120:340–352. [PubMed: 17200142]

Spiess MR, Müller RM, Rupp R, Schuld C, van Hedel HJ, EM-SCI Study Group. Conversion in ASIA impairment scale during the first year after traumatic spinal cord injury. J Neurotrauma. 2009; 26:2027–2036. [PubMed: 19456213]

Stam FJ, MacGillavry HD, Armstrong NJ, de Gunst MC, Zhang Y, van Kesteren RE, Smit AB, Verhaagen J. Identification of candidate transcriptional modulators involved in successful regeneration after nerve injury. Eur J Neurosci. 2007; 25:3629–3637. [PubMed: 17610582]

Starkey ML, Barritt AW, Yip PK, Davies M, Hamers FP, McMahon SB, Bradbury EJ. Assessing behavioural function following a pyramidotomy lesion of the corticospinal tract in adult mice. Exp Neurol. 2005; 195:524–539. [PubMed: 16051217]

Starkey ML, Bartus K, Barritt AW, Bradbury EJ. Chondroiti-nase ABC promotes compensatory sprouting of the intact corticospinal tract and recovery of forelimb function following unilateral pyramidotomy in adult mice. Eur J Neurosci. 2012; 36:3665–3678. [PubMed: 23061434]

Swaney JS, Chapman C, Correa LD, Stebbins KJ, Broadhead AR, Bain G, Santini AM, Darlington J, King CD, Baccei CS, et al. Pharmacokinetic and pharmacodynamic characterization of an oral lysophos-phatidic acid type 1 receptor-selective antagonist. J Pharmacol Exp Ther. 2011; 336:693–700. [PubMed: 21159750]

Trapnell C, Hendrickson DG, Sauvageau M, Goff L, Rinn JL, Pachter L. Differential analysis of gene regulation at transcript resolution with RNA-seq. Nat Biotechnol. 2013; 31:46–53. [PubMed: 23222703]

Tuszynski MH, Steward O. Concepts and methods for the study of axonal regeneration in the CNS. Neuron. 2012; 74:777–791. [PubMed: 22681683]

Velmans T, Battefeld A, Geist B, Farrés AS, Strauss U, Bräuer AU. Plasticity-related gene 3 promotes neurite shaft protrusion. BMC Neurosci. 2013; 14:36. [PubMed: 23506325]

Verhaagen J, Van Kesteren RE, Bossers KA, Macgillavry HD, Mason MR, Smit AB. Molecular target discovery for neural repair in the functional genomics era. Handb Clin Neurol. 2012; 109:595–616. [PubMed: 23098739]

Wang Z, Reynolds A, Kirry A, Nienhaus C, Blackmore MG. Overexpression of Sox11 promotes corticospinal tract regeneration after spinal injury while interfering with functional recovery. J Neurosci. 2015; 35:3139–3145. [PubMed: 25698749]

Zhang Y, Chen K, Sloan SA, Bennett ML, Scholze AR, O'Keeffe S, Phatnani HP, Guarnieri P, Caneda C, Ruderisch N, et al. An RNA-sequencing transcriptome and splicing database of glia, neurons, and vascular cells of the cerebral cortex. J Neurosci. 2014; 34:11929–11947. [PubMed: 25186741]

Zou Y, Stagi M, Wang X, Yigitkanli K, Siegel CS, Nakatsu F, Cafferty WB, Strittmatter SM. Gene-silencing screen for mammalian axon regeneration identifies Inpp5f (Sac2) as an endogenous suppressor of repair after spinal cord injury. J Neurosci. 2015; 35:10429–10439. [PubMed: 26203138]

Highlights

- Mechanisms driving functional plasticity of intact CNS circuits are unknown
- Retrograde spinal tracing reveals CST neurons undergoing functional plasticity
- Transcriptional profiling of these neurons reveals pro-axon growth targets
- Molecular modulation of the identified LPA-LPPR1 axis enhances plasticity post-SCI

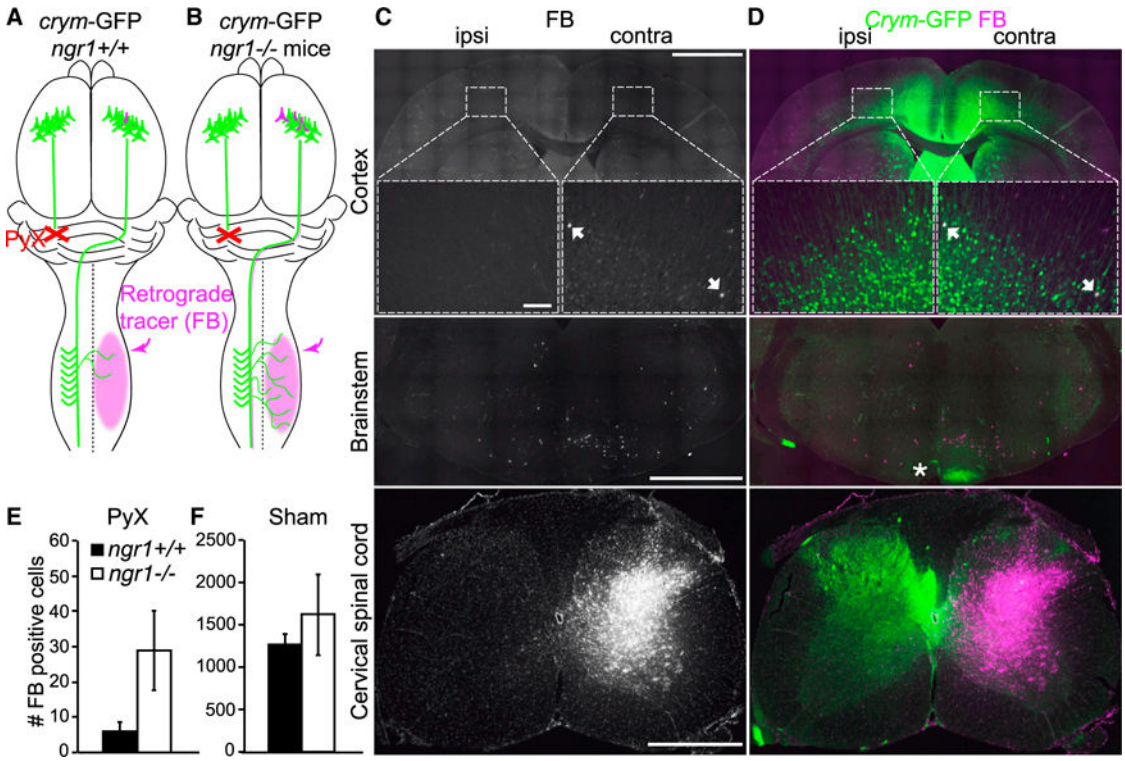

Figure 1. Spinal Retrograde Labeling Identifies Intact Sprouting CSMNs after PyX

Schematics show retrograde CSMN labeling via intraspinal infusion of FB (magenta) in *ngr1*$^{+/+}$ (A) and *ngr1*$^{-/-}$ (B) Crym-GFP mice after PyX (red X). No GFP^{+} CSMNs were retrogradely labeled with FB in ipsi (to the PyX) cortex in *ngr1*$^{-/-}$ mice (C) after PyX. Intact sprouting FB^{+} (C and D, inset arrows) GFP^{+} CSMNs were seen in contra cortex 4 weeks post-PyX due to FB uptake by intact sprouting CST axons (B). Intact crossed reticulospinal tract axons accumulate FB dorsal to the PyX confirming efficiency of FB transport (C and D). The absence of crym-GFP in the left pyramid confirms complete unilateral CST ablation (D, asterisk). FB infusion diffuses dorso-ventrally, but remains unilateral (C and D). *Crym*-GFP^{+} CST axons can be seen sprouting in the tracer enriched denervated side of the spinal cord (D). Significantly more *crym*-GFP^{+} CST axons sprouted in the denervated spinal cord in *ngr1*$^{-/-}$ compared to *ngr1*$^{+/+}$ mice (see also Figures S2A–S2G), and accordingly elevated numbers ($p = 0.07$, Student's t test) of sprouting (FB^{+}GFP^{+}) CSMNs were observed in contra cortex of *ngr1*$^{-/-}$ compared to *ngr1*$^{+/+}$ mice (E). The number of ipsi CSMNs labeled after sham lesion was invariant between *ngr1*$^{-/-}$ and *ngr1*$^{+/+}$ mice (F; data are presented as the average of the total number of FB+ cells counted per animal ± SEM). Scale bars, 100 and 500 μm.

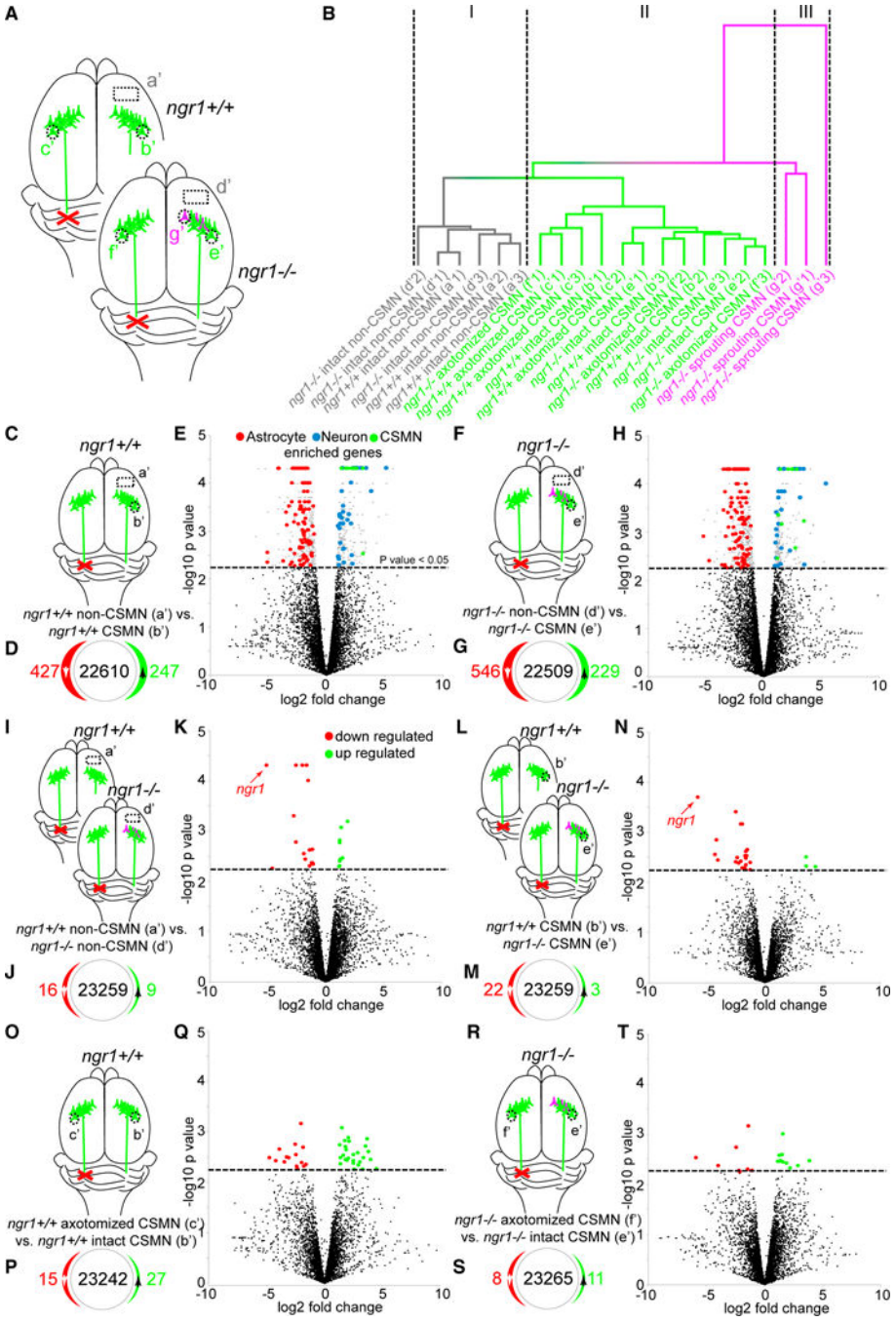

Figure 2. Intact Sprouting CSMNs Display Unique Expression Profile

(A and B) We used LCM to extract RNA (A) from non-CSMNs (a′), intact quiescent CSMNs (b′), axotomized CSMNs (c′) from crym-GFP *ngr1*$^{+/+}$ mice, non-CSMNs (d′), intact quiescent CSMNs (e′), axotomized CSMNs (f′), and intact sprouting CSMNs (g′) from crym-GFP *ngr1*$^{-/-}$ mice 4 weeks after PyX (n = 3/genotype) for differential transcriptional profiling. Replicate samples (n = 3) clustered into three groups (B).

(C and D) Comparing samples a′ versus b′ (C) showed that 427 genes were downregulated and 247 upregulated (D, 22,610 remained unchanged) in intact quiescent CSMNs compared to non-CSMNs in *ngr1*$^{+/+}$ mice.

(E–G) Volcano plot shows every gene profiled as log2 fold change versus–log10 of the false discovery rate (FDR) corrected p value. Non-SDE genes (black dots) are separated from SDE genes (gray dots) by $p < 0.05$ cut off (stippled) line. Intact quiescent CSMNs (b′) are enriched in neuronal (blue dots) and CSMN-specific genes (green dots) and show a dearth in expression of astrocytic genes compared to non-CSMNs (a′). Similarly, comparing samples d′ versus e′ (F), show that 546 genes were downregulated and 229 upregulated (G, 22,509 remained unchanged) in intact quiescent CSMNs compared to non-CSMNs in *ngr1*$^{-/-}$ mice.

(H) Volcano plot shows *ngr1*$^{-/-}$ CSMNs were also enriched in neuronal and CSMN-specific genes and showed paucity in expression of astrocytic genes (red dots).

(I and J) Comparing non-CSMNs between genotypes (I, a′ versus d′) showed that only 16 genes were downregulated and 9 upregulated (J, 23,259 remained unchanged) in non-CSMNs from *ngr1*$^{-/-}$ versus to *ngr1*$^{+/+}$ mice.

(K–M) Volcano plot (K) shows all profiled genes, *ngr1* (labeled) is the most downregulated. Comparing CSMNs between genotypes (schematic L, b′ versus e′) showed that only 22 genes were downregulated and 3 upregulated (M, 23,259 remained unchanged) in *ngr1*$^{-/-}$ versus *ngr1*$^{+/+}$ mice.

(N–P) Volcano plot (N) shows all profiled genes, *ngr1* (labeled), is the most downregulated. Comparing samples c′ versus b′ (O) showed that 15 genes were downregulated and 27 genes upregulated (P, 23,242 remained unchanged) in intact quiescent CSMNs samples versus axotomized CSMNs in *ngr1*$^{+/+}$ mice.

(Q–S) Volcano plot (Q) shows all genes profiled. Comparing samples f′ versus e′ (R) showed that 8 genes were downregulated and 11 upregulated (S, 23,256 remained unchanged) in intact quiescent CSMNs versus axotomized CSMNs in *ngr1*$^{-/-}$ mice.

(T) Volcano plot shows all genes profiled.

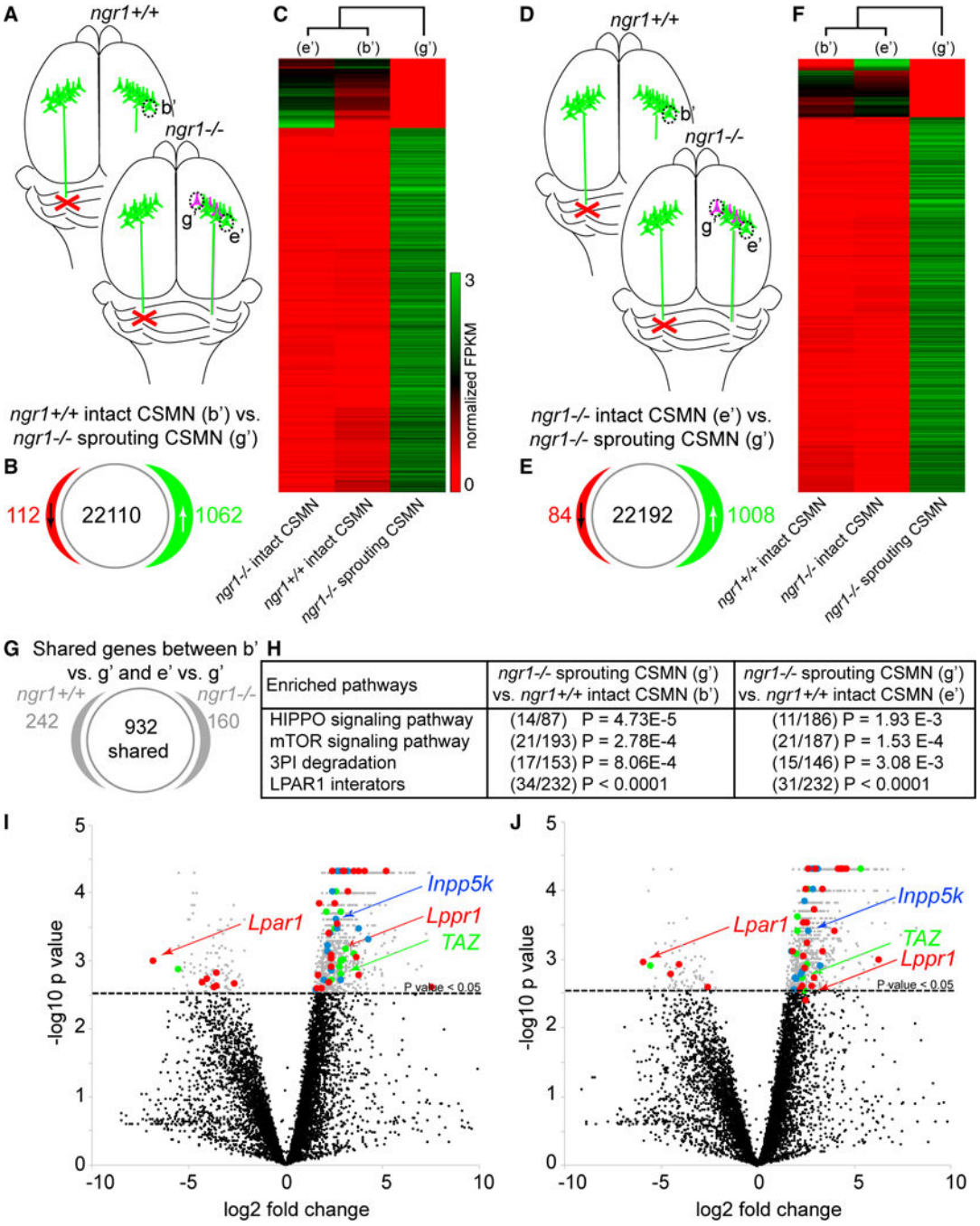

Enriched pathways	*ngr1-/-* sprouting CSMN (g') vs. *ngr1+/+* intact CSMN (b')	*ngr1-/-* sprouting CSMN (g') vs. *ngr1+/+* intact CSMN (e')
HIPPO signaling pathway	(14/87) P = 4.73E-5	(11/186) P = 1.93 E-3
mTOR signaling pathway	(21/193) P = 2.78E-4	(21/187) P = 1.53 E-4
3PI degradation	(17/153) P = 8.06E-4	(15/146) P = 3.08 E-3
LPAR1 interators	(34/232) P < 0.0001	(31/232) P < 0.0001

Figure 3. Comparing Intact Sprouting with Intact Quiescent CSMNs Reveals Plasticity-Related Genes

(A–H) Comparing samples b′ and g′ (A) showed that 112 genes were downregulated and 1,062 were upregulated in intact sprouting CSMNs from *ngr1*$^{-/-}$ mice versus intact quiescent CSMNs from *ngr1*$^{+/+}$ mice (B, 22,110 remained unchanged). Heatmap (C) of normalized fragments per kilobase of transcript per million mapped reads (FPKM) of the 1,174 SDE genes comparing intact quiescent CSMNs from *ngr1*$^{+/+}$ to intact sprouting CSMNs from *ngr1*$^{-/-}$ (A, b′ versus g′) confirms that intact quiescent CSMN samples cluster across genotypes (e′ and b′) and more distantly from intact sprouting CSMNs (g′).

Similarly, comparing gene expression profiles between samples e′ and g′ (D) showed that 84 genes were downregulated and 1008 were upregulated in intact sprouting CSMNs from *ngr1*$^{-/-}$ mice compared to intact quiescent CSMNs from *ngr1*$^{-/-}$ mice (E, 22,192 remained unchanged). Heatmap (F) of normalized FPKMs of the 1,092 SDE genes comparing intact quiescent CSMNs from *ngr1*$^{-/-}$ to intact sprouting CSMNs from *ngr1*$^{-/-}$ (D, e′ versus g′), again confirms that intact quiescent CSMNs cluster across genotypes (b′ and e′) and more distantly from intact sprouting CSMNs (g′). Seventy percent of SDE genes (932 genes) were shared between these two comparisons (G). IPA revealed the top pathways (H, Fisher's exact test, number of SDE genes/total number in pathway, LPAR1 interactors Chi-square test) enriched in sprouting CSMN samples from *ngr1*$^{-/-}$ mice compared to intact quiescent CSMN samples from *ngr1*$^{+/+}$ (g′ versus b′) and *ngr1*$^{-/-}$ samples (g′ versus e′).
(I and J) Volcano plots displays the log2 fold change versus –log10 of the false discovery rate (FDR) corrected p value of every gene profiled comparing intact sprouting CSMNs from *ngr1*$^{-/-}$ mice versus intact quiescent CSMNs from *ngr1*$^{+/+}$ mice (I, samples g′ versus b′) and *ngr1*$^{-/-}$ (J, samples g′ versus e′). Select pathways are highlighted (red, SDE LPAR1 interactors; blue, SDE 3-phosphoinositide signaling pathway genes; green, SDE hippo signaling pathway genes; gray, other SDE genes; black, non SDE genes) and candidate genes *(Lpar1, Lppr1, Inpp5k, TAZ)* were selected for functional analysis.

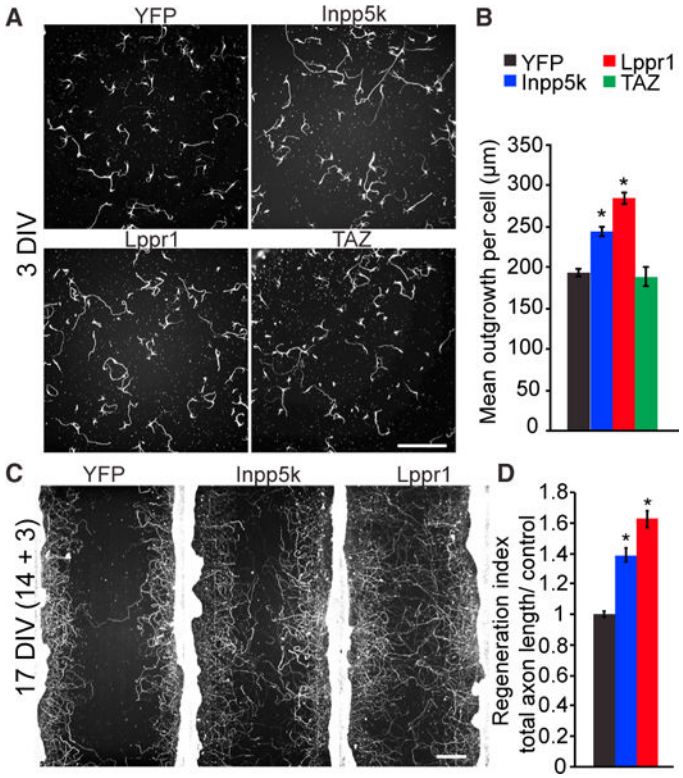

Figure 4. Overexpression of LPPR1 and INPP5K Significantly Enhances Cortical Axon Growth In Vitro

Wild-type E17 cortical neurons overexpressing YFP control or genes of interest (A). Overexpression of INPP5K and LPPR1 resulted in a significant increase in mean outgrowth per cell after 3 DIV (B, *p < 0.0001, one-way ANOVA followed by Dunnett's post hoc test). Data are shown as mean outgrowth per cell ± SEM, averaged over four sites per 96-well culture plate from three biological replicates (n = 62–69 wells per condition). To model neurite growth after an in vitro injury, E17 neurons were transduced with AAV-*YFP*, AAV-*Inpp5k*, or AAV-*Lppr1* (C). After 14 DIV culture wells were scraped with a pin replicator. Neurons overexpressing YFP exhibited minimal regeneration into the scrape zone (C). Overexpression of INPP5K or LPPR1 resulted in a significant increase in regeneration (C and D, *p < 0.0001, one-way ANOVA followed by Dunnett's post hoc test). Data are presented as the average regeneration index per well ± SEM. Scale bars, 100 μm.

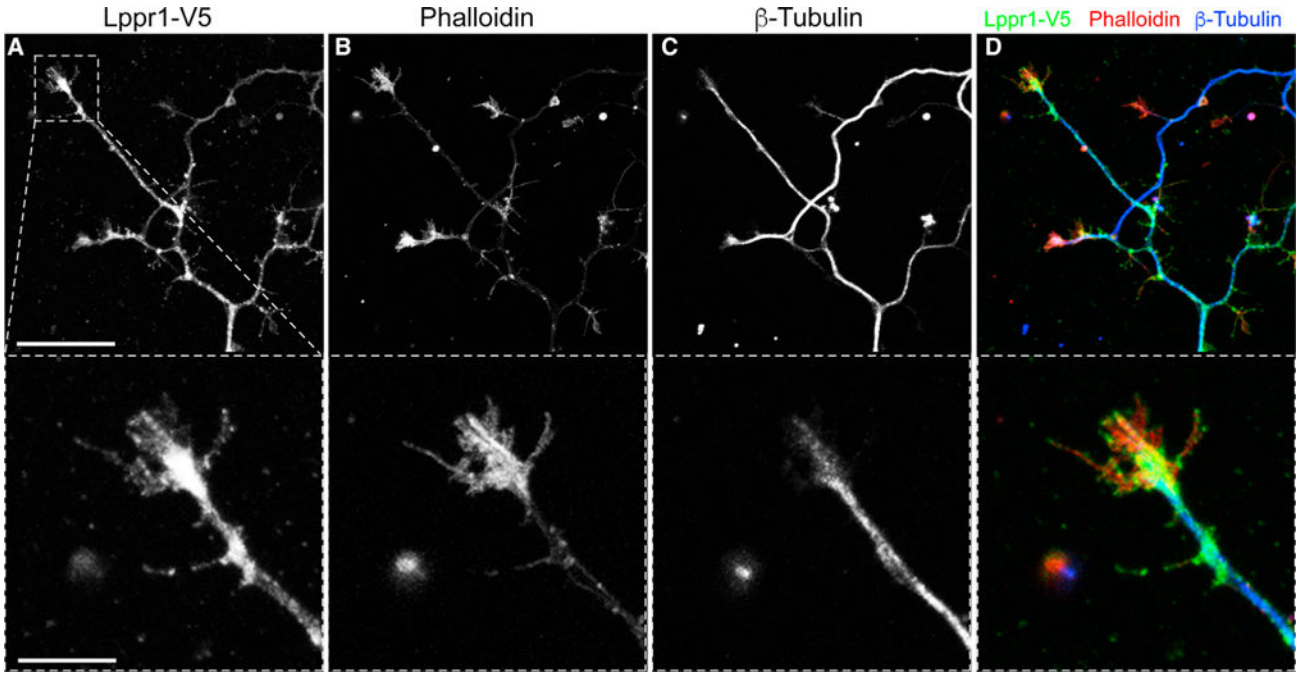

Figure 5. LPPR1 Accumulates in Cortical Neuron Growth Cones In Vitro

LPPR1-V5 was overexpressed in E17 cortical neurons. After 7 DIV, LPPR1-V5 can be seen localizing to the neurite shaft and accumulating in Phalloidin rich spiny outgrowths protruding from the neurite shaft (A–D). Higher power insets show LPPR1-V5 accumulating in the leading edge and body of growth cones (V5, green; Phalloidin, red; β-tubulin, blue). Scale bars, 25 and 5 μm.

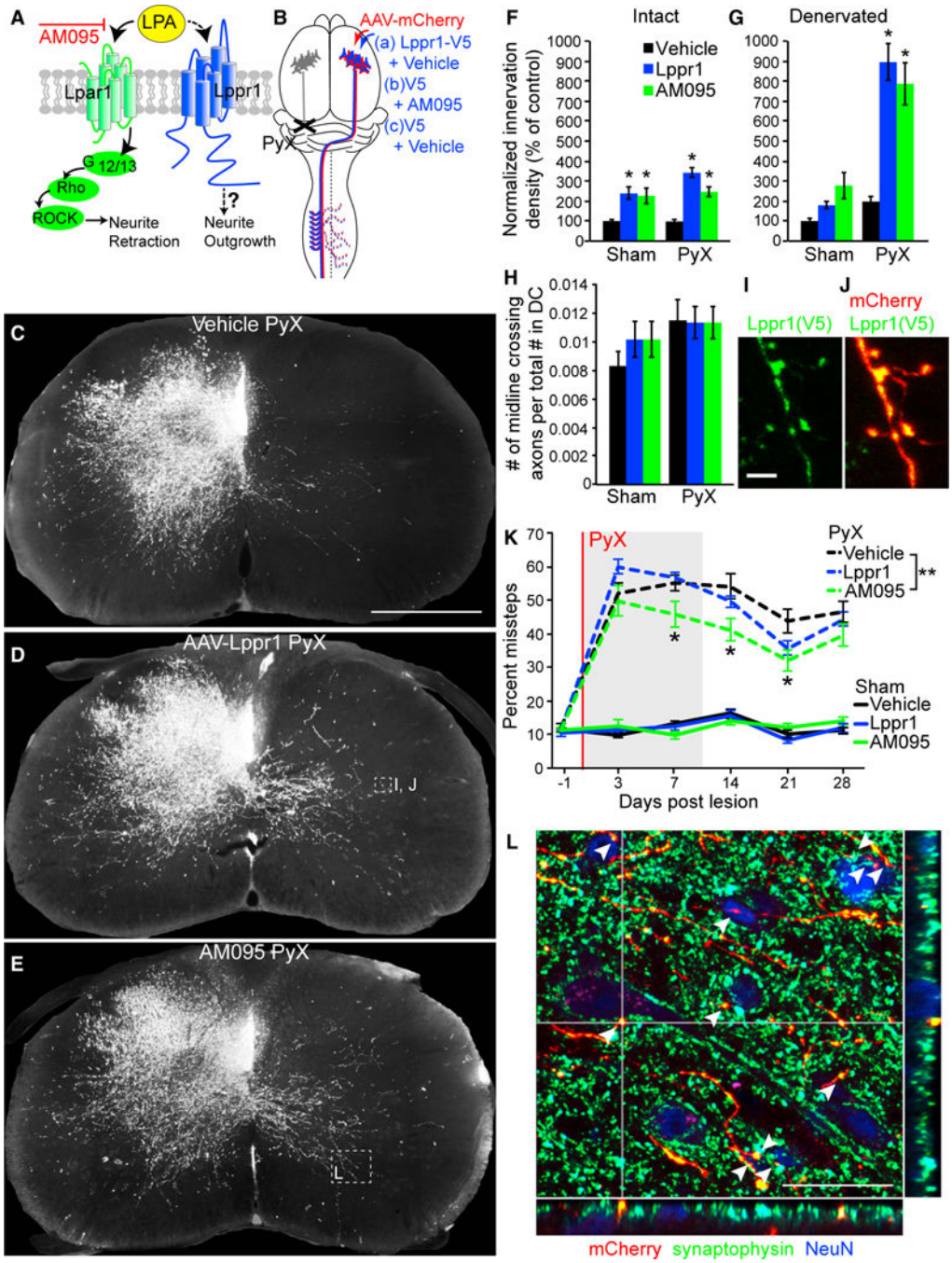

Figure 6. Modulating LPA-LPAR1 Binding Enhances Functional Plasticity after PyX

Schematic (A) shows a role for LPPR1/LPAR1 in modulating LPA signaling. LPAR1 is a G protein-coupled receptor for LPA. Once bound, LPA activates Rho/ROCK via $G_{12/13}$ to induce growth cone collapse and neurite retraction (Kranenburg et al., 1999). LPPR1 is a membrane-spanning protein that may activate neurite outgrowth via an LPAR1-independent mechanism (Savaskan et al., 2004). LPA binding to LPAR1 is blocked with the LPAR1-specific antagonist AM095 (Swaney et al., 2011). We used two strategies to relieve the block of LPA signaling on axon growth in vivo, via either viral overexpression of LPPR1 in

CSMNs or systemic delivery of the AM095 (B). Adult wild-type mice received either PyX or sham lesion 2 weeks after cortical infusion of either AAV-*Lppr1-V5* (Ba) or AAV-*V5* (Bb, Bc), and all mice received AAV-mCherry to label the CST. Five hours post-lesion, mice began a 10-day, 2×/day, oral treatment with AM095 (Bb) or vehicle (Ba, Bc). Four weeks post-lesion, control PyX mice (AAV-*V5* + vehicle, n = 8, C) showed no difference in the innervation of mCherry$^+$ CST axons in the intact (F, data are presented as the average innervation density across all mice in the group divided by the average innervation density from the vehicle sham group ± SEM) and denervated ventral horn (G) in comparison to control sham mice (n = 8). LPPR1-expressing (AAV-*Lpp/1 -V5* + vehicle, n = 15, D) and AM095-treated (AAV-*V5* + AM095, n = 8, E) mice showed a significant increase in the density of mCherry$^+$ CST axons into both the intact (F, *$p < 0.001$, one-way ANOVA followed by Dunnett's post hoc test) and denervated (G, *$p < 0.0001$, one-way ANOVA followed by Dunnett's post hoc test) ventral horns after PyX in comparison to vehicle-treated sham-lesioned controls. LPPR1-expressing (n = 6) and AM095-treated (n = 6) mice also showed a significant increase in the density of mCherry$^+$ CST axons in the intact ventral horn (D, *$p < 0.001$, one-way ANOVA followed by Dunnett's post hoc test) and a trend toward an increase in the denervated ventral horns (E) after sham lesion, demonstrating an injury-independent increase in intact CST sprouting. There was no significant difference in the number of mCherry$^+$ CST axons that crossed the midline in any group (H, one-way ANOVA followed by Dunnett's post hoc test). V5 staining showed that LPPR1 (I and J) was co-localized with mCherry$^+$ CST axons that were sprouting in the denervated ventral horn. Grid-walking analysis showed that PyX-lesioned mice exhibited a significant contra impairment post-lesion (K, stippled lines, data are shown as the average percentage fore and hind limb missed steps within each group ± SEM, PyX denotes time of lesion, shading denotes duration of drug/vehicle treatment). AM095-treated mice recovered significant function in comparison to vehicle-treated control mice after PyX (K, **$p < 0.05$, one-way ANOVA with repeated measures, *$p < 0.05$ post hoc ANOVA). LPPR1-expressing mice showed a trend toward recovery, however, this did not reach significance. There was no significant difference in grid walking behavior after treatment between sham-lesioned mice (I, solid lines). Photomicrograph (L) shows mCherry (red), synaptophysin (green), and NeuN (blue) staining in a C8 ventral spinal cord section showing the presence of synaptic puncta (white arrowheads) on CST axons in close apposition with ventral horn neurons. Scale bars, 500 μm (C); 10 μm (I); 100 μm(L).

Table 1

Significantly Differentiated Genes from the LPAR1, 3-Phosphoinositide Degradation, HIPPO, and mTOR Pathways

Gene	Versus Intact *ngr*$^{+/+}$	Versus Intact *ngr*$^{-/-}$
LPAR1 Interactors		
Abcc4	4.94	10.59
Adora2b	105.10	21.39
Adra2c	8.59	10.82
Adrb2	195.47	81.80
Colec12	5.15	7.87
Csf2ra	9.95	8.06
E2f4	5.08	5.25
Enpp4	↓ 11.61	↓7.95
Gab2	14.30	14.21
Golga5	8.37	8.38
Gpr153	13.22	7.16
Gpr176	↓ 12.34	↓16.15
Gpr75	18.12	22.10
Gpr83	14.53	25.79
Grm2	5.44	5.43
Hmgcr	5.49	6.46
Htr2c	38.06	20.79
Irs2	5.47	4.80
Lgr4	14.17	20.49
Lppr1	9.32	5.94
Lpar1	↓ 109.57	↓57.58
Mapk6	5.47	6.17
Mapk7	4.99	5.72
Ntsr1	↓ 18.88	↓21.44
Ociad1	3.19	2.69
Oprl1	4.97	5.94
Pdia3	3.40	3.74
Pigo	12.15	18.64
Pik3cb	6.60	6.08
Plcb4	↓6.09	↓5.78
Rgs4	3.52	2.78
Rtn2	3.82	3.57
S1pr5	↓ 16.02	↓ 10.62
Scap	6.17	5.45
Slc30a7	↓ 11.31	↓9.23

Gene	Versus Intact *ngr*$^{+/+}$	Versus Intact *ngr*$^{-/-}$
Smad3	6.18	7.88
Smad4	7.48	6.07
Trhr	14.10	16.41
3-Phosphoinositide Degradation Pathway		
Dusp1	5.32	5.02
Figure 4	8.14	7.42
Igbp1	5.11	9.19
Inpp5j	9.81	7.58
Inpp5k	6.35	7.51
Nudt15	7.65	7.97
Ocrl	6.57	5.26
Ppapdc3	7.76	4.88
Ppp1r13b	4.62	5.53
Ppp2r5b	4.69	4.10
Ppp2r5e	6.51	4.39
Ptpn13	20.04	6.93
Rasa1	7.23	6.32
Synj1	3.13	3.54
Thtpa	14.32	10.04
Ublcp1	4.11	3.91
Wbp11	5.60	3.93
Dusp1	5.32	5.02
HIPPO Pathway		
Cd44	7.68	5.64
Csnk1d	5.25	5.22
Dlg1	6.44	6.40
Ppp1r14c	8.92	4.28
Ppp1r3d	12.04	7.35
Ppp2r5b	4.69	4.10
Ppp2r5e	6.51	4.39
Prkcz	4.54	4.28
Rassf1	↓ 45.02	↓45.31
Smad3	6.18	7.88
Smad4	7.48	6.07
Tead1	8.38	41.88
Tjp2	7.13	4.17
Wwtr1	7.48	5.71
mTOR Signaling		
Atg13	4.61	4.20

Gene	Versus Intact *ngr*$^{+/+}$	Versus Intact *ngr*$^{-/-}$
Ddit4	18.87	12.04
Dgkz	3.41	3.44
Eif3b	4.57	4.83
Eif3e	3.22	4.00
Eif3m	3.47	3.57
Eif4ebp1	21.66	8.40
Eif4g2	3.67	4.41
Fkbp1a	3.27	2.90
Napepld	11.47	11.72
Pik3cb	6.60	6.08
Pik3r3	4.41	4.96
Pld2	3.85	8.74
Pld4	11.58	6.38
Ppp2r5b	4.69	4.10
Ppp2r5e	6.51	4.39
Prkch	425.24	53.32
Prkci	↓ 10.99	↓8.82
Prkcz	4.54	4.28
Prkd1	13.50	15.48
Rhoc	8.15	4.32
Rhot1	4.23	5.11
Rhou	6.79	8.50
Rps19		
Rps25	3.72	2.75
Rps6	3.14	2.97

Genes significantly differentially expressed between *ngr1*$^{-/-}$ intact sprouting CSMNs versus intact quiescent CSMNs from *ngr1*$^{+/+}$ and *ngr1*$^{-/-}$ mice from the LPAR1, 3-phosphoinositide degradation, HIPPO, and mTOR pathways. Fold change for each comparison is listed per gene (↓, downregulated genes).